



**HAL**  
open science

# Combined Temperature and Humidity Chipless RFID Sensor

Florian Requena, Nicolas Barbot, Darine Kaddour, Etienne Perret

► **To cite this version:**

Florian Requena, Nicolas Barbot, Darine Kaddour, Etienne Perret. Combined Temperature and Humidity Chipless RFID Sensor. *IEEE Sensors Journal*, 2022, 22 (16), pp.16098-16110. 10.1109/JSEN.2022.3189845 . hal-03775002

**HAL Id: hal-03775002**

**<https://hal.science/hal-03775002v1>**

Submitted on 12 Sep 2022

**HAL** is a multi-disciplinary open access archive for the deposit and dissemination of scientific research documents, whether they are published or not. The documents may come from teaching and research institutions in France or abroad, or from public or private research centers.

L'archive ouverte pluridisciplinaire **HAL**, est destinée au dépôt et à la diffusion de documents scientifiques de niveau recherche, publiés ou non, émanant des établissements d'enseignement et de recherche français ou étrangers, des laboratoires publics ou privés.

# Combined Temperature and Humidity Chipless RFID Sensor

Florian Requena, *Student Member, IEEE*, Nicolas Barbot, *Member, IEEE*,  
Darine Kaddour, *Member, IEEE*, and Etienne Perret, *Senior Member, IEEE*

**Abstract**—A temperature and humidity chipless RFID sensor is presented in this paper. The tag ID as well as the two physical parameters are extracted using a traditional chipless RFID tag and interrogation procedure. No specific material, i.e. particularly sensitive to the quantities to be measured, is used for ease of implementation. The method is based on a model which describes precisely the evolution of the scatterer’s resonance frequency as a function of temperature and humidity. The materials permittivity (impacted by these two quantities) and dilatation (impacted only by the temperature) are taken into consideration to estimate these two physical quantities independently and simultaneously using only the measurement of the resonance frequencies of two scatterers. Measurements in a controlled environment and in a real environment are achieved showing the potential of this approach for the sensor application. The sensing limitation as well as the possibility of this approach to characterize the temperature and humidity dependencies of unknown materials are also presented.

**Index Terms**—Humidity sensor, radar, scatterer, temperature sensor, wireless measurement.

## I. INTRODUCTION

CHIPLESS RFID is an identification technology that produces tags similar to barcodes using a wireless radar approach [1]. Numerous RFID families have emerged to address new challenging issues. Chipless RFID is an example; the objective is to reduce considerably the price of the tag to compete with the barcode by removing the electronic parts [2]. In recent years, this technology has undergone a considerable expansion both in its applications and in its associated research efforts. Several works can be found on coding capacity [3]–[5], reading robustness [6], [7] or inkjet printing techniques [8]. While the overall price of a chipless tag can not be reduced to perfectly match that of the barcode, the functionalities that its competitor does not have are put forward. We find assets linked to its reading method based on EM waves but also the possibility to add sensor functionalities directly to the tag [9]–[11]. Several chipless RFID humidity sensors have been published [12]–[14]. In these works, dedicated substrates with permittivities sensitive to humidity are used. In this case, a humidity variation will cause a variation of the permittivity detected by resonators resulting in a shift of their resonance frequencies. These frequency shifts are used to compute the ambient humidity around the resonator. At the same time, multiple chipless RFID temperature sensors have been made [15]–[18] based on the same idea, i.e. temperature variations induce

a shift on the resonance frequency which can be detected by the reading system. The link between the resonant frequency and temperature involves two physical phenomena. The first studied mechanism is the thermal expansion of the material. In this case, when the temperature varies, the physical dimensions of the resonator will change resulting in a variation of the resonance frequency. The second mechanism is the change of the dielectric constant of the substrate with the temperature. Similar phenomena is observed for humidity. One of the advantages highlighted with this remote reading approach is the possibility to retrieve the tag identifier (ID) along with the temperature even through some everyday objects, such as through a wall or a door [18]. A summary of recent works is presented in Table I.

An important limitation of these works is that these sensors can only estimate a single physical parameter while the other has to remain constant (and known). However, in a real-life application, both temperature and humidity will vary and impact the resonance frequency which is used as a sensor but also to decode the tag identifier. This is due to the fact that most of these studies are not based on an analytical model. Indeed they use an empirical approach, which makes it impossible to separate the effects of temperature and humidity. Note that these two variables have an impact on the resonance frequency, which is generally the only quantity that is measured and therefore used to recover the information related to these two independent quantities. Then, when humidity is studied for example, temperature variation can be wrongly interpreted introducing errors on the extracted humidity. Therefore, the real-world applicability of these sensors is debatable. Also, contrary to the majority of works on chipless sensors where specific materials are used to obtain the desired function, the introduced approach is based on an analytical model and can be simply applied to tags previously introduced for identification applications. These tags do not contain any specific material, i.e. particularly sensitive to the quantities to be measured and they have the advantage of being simple to manufacture. An undeniable advantage over other works is the ability to simultaneously retrieve three independent information sources : the tag identifier, the surrounding temperature and humidity. In [19] the authors introduced a method for sensing both temperature and humidity at the same time with a chipless RFID approach. While based on the original idea of [19], this paper redrafts the problem definition from a theoretical point of view and goes as far as showing the potential and the limits of this approach through several practical experiments. Thus, this paper shows how to measure two physical quantities at the

The authors are with Univ. Grenoble Alpes, Grenoble INP, LCIS, F-26000 Valence, France.

E. Perret is also with Institut Universitaire de France, Paris, France.

same time without the addition of any specific material, with a very accurate physical model that predicts the evolution of the resonance frequency of resonators when the tag is subjected to both temperature and humidity variations. Measurements in a real environment; a study of repeatability on the extraction of the physical quantities and their limiting range, as well as Monte-Carlo simulations are achieved in this paper. A method to characterize the temperature and humidity dependencies of unknown materials is also proposed. This paper focuses on the estimation of temperature and humidity based on the chipless RFID technology. The study of the remote sensing principle through obstacles (wood, glass, walls...), reading distance or resonator geometry has already been presented in detail in [18]. As the obtained results showed good performance in reading, these studies have not been repeated here.

The paper is organized as follows, Section II introduces the expressions used to extract the temperature and humidity from the measured S-parameters. In Section III, simulations are presented to validate this method. Section IV and Section V illustrate measurements in a controlled and in a real environment respectively. Section VI presents a method to estimate the model coefficients, a repeatability study and the estimation of the errors and the uncertainties of the method using Monte-Carlo simulations. Finally, Section VII concludes the paper.

## II. THEORY

### A. Relationship between resonance frequency, temperature and humidity

The measurement principle used, based on a radar approach, is illustrated in Fig. 1. In this paper, the chipless RFID sensor considered is a loop resonator (see Fig. 1) but the approach can be generalized to other resonator shapes. When a loop resonator is illuminated by an incoming EM-field (see Fig. 1), the maximum energy back-scattered at a temperature  $T$  and relative humidity  $RH$  occurs at its resonant frequency  $f$  defined by radar approach measurement [25]:

$$f(T, RH) = \frac{c}{2\sqrt{\varepsilon_{eff}(T, RH)}L(T)} \quad (1)$$

where  $c$  is the speed of light in vacuum,  $\varepsilon_{eff}(T, RH)$  is the effective permittivity seen by the loop and  $L(T)$  the effective length of the loop resonator as defined in [25]. The thermal dependence of the tag geometry  $L(T)$  is due to the thermal expansion and can be expressed with [26] :

$$L(T) = L_0(1 + \alpha_c T) \quad (2)$$

where  $\alpha_c$  is the equivalent expansion coefficient for the effective length and  $L_0$  the effective length of the loop at  $T = 0^\circ\text{C}$ . Note that the relation between this effective length  $L$  and the physical length  $l$  of the loop (see Fig. 1) will be clarified later in this section. As previously said in the introduction, in the most general case, the substrate dependence of humidity is unknown but by considering small variations of humidity around a specific value  $RH_0$ , where  $RH$  denotes the relative humidity (in %) seen by the resonator, it is possible to linearize

the resonator substrate permittivity  $\varepsilon_r$  with:

$$\varepsilon_r(T, RH) \simeq \varepsilon_r(RH)(1 + \beta T) \simeq \varepsilon_r(RH_0)(1 + \beta T) \times \left[ 1 + \frac{\varepsilon'_r(RH_0)}{\varepsilon_r(RH_0)}(RH - RH_0) \right] \quad (3)$$

where  $\beta$  is the thermal dependence of the substrate often characterized by the provider.  $\varepsilon'_r(RH_0)$  is the derivative of  $\varepsilon_r$  according to the variable  $RH$ . Equation (3) can be rewritten as:

$$\varepsilon_r(T, RH) = \varepsilon_r(RH_0)(1 + \beta T)(1 + [a + \eta RH]). \quad (4)$$

The coefficients  $a$  and  $\eta$  represent the humidity dependence of the substrate. For the loop, the effective permittivity can be modelled by considering the resonator as a slot line terminated at both ends by a short circuit (SC) [25]. Thus, the effective permittivity of the loop resonator  $\varepsilon_{eff}$ , on a single substrate layer, can be expressed as [27] :

$$\varepsilon_{eff}(T, RH) = 1 + \frac{\varepsilon_r(1 + \beta T)(1 + [a + \eta RH]) - 1}{2} q \quad (5)$$

where  $\varepsilon_r$  is the permittivity of the substrate at  $T = 0^\circ\text{C}$  and  $RH = RH_0$ . The parameter  $q$  is dependent on the thickness of the substrate and the geometry of the resonator as described by the analytical expression given in [27, eq. (21)] which leads to :

$$\varepsilon_{eff}(T, RH) \simeq \varepsilon_{eff}(0, RH_0)(1 + \alpha_p T)(1 + a' + \gamma RH) \quad (6)$$

with :

$$\alpha_p = \frac{\beta q \varepsilon_r}{2 + (\varepsilon_r - 1)q} \quad (7)$$

and

$$\gamma = \frac{\eta q \varepsilon_r}{2 + (\varepsilon_r - 1)q} \quad (8)$$

and

$$a' = \frac{a q \varepsilon_r}{2 + (\varepsilon_r - 1)q} \quad (9)$$

In this case, (1) can be rewritten as :

$$f(T, RH) = \frac{c}{2\sqrt{\varepsilon_{eff}(1 + \alpha_p T)(1 + a' + \gamma RH)}L_0(1 + \alpha_c T)} \simeq F \times (1 - \alpha T - \frac{1}{2}[a' + \gamma RH]) \quad (10)$$

with

$$\alpha = \alpha_c + \alpha_p/2 \text{ and } F = \frac{c}{2\sqrt{\varepsilon_{eff}}L_0} \quad (11)$$

Notice that the thermal and humidity dependence on the permittivity is expressed by the coefficients  $\alpha$ ,  $a'$  and  $\gamma$  in (10). For this reason, the value of  $\varepsilon_{eff}$  in (10) is a constant which does not depend on the temperature nor on the humidity. Please also note that for the remainder of this section, we will consider the values of  $\alpha$ ,  $a'$  and  $\gamma$  to be known. A method for the extraction (used in the measurement part of the paper) of these coefficients will be described later in the paper (in section VI).

The principle of the sensor introduced in this article is based on the use of two resonators of the same topology. Rectangular loop resonators are studied for their good EM performance.

TABLE I  
COMPARISON OF CHIPLESS AND ANTENNA-BASED TEMPERATURE OR HUMIDITY SENSORS

Article	Sensing parameter	Effect investigated	Materials considered	Measurements in real environment	Sensor design
[15]	Temperature	Change in permittivity	Stanyl polyamide	No	Planar shape – PCB design
[17]	Temperature	Change in permittivity	Stanyl polyamide	Not mentioned	Planar shape – PCB design
[20]	Temperature	Change in conductivity	Polymer carbon nanotube composite ink	No	Planar shape – inkjet printed
[21]	Temperature	Dilatation of 3D structure	Gold and silver cantilever	Yes	3D cantilever – Clean room
[22]	Temperature	Change in permittivity	Ceramic cylinder	Yes	Fully dielectric machined
[23]	Humidity	Change in permittivity	Kapton HN polyamide	Yes	Planar shape – inkjet printed
[12]	Humidity	Change in permittivity	PVA polymer	No	Planar shape
[13]	Humidity	Change in permittivity	PET film	No	Planar shape – inkjet printed
[24]	Humidity	Change in permittivity	Silicon nanowires	No	Planar shape – PCB design
*	Temperature & Humidity	Change in permittivity & dilatation	Metallic resonator on a RO4003C substrate without materials particularly sensitive to $T$ & $RH$	Yes	Planar shape – PCB design

\* This paper

As illustrated in Fig. 1, the resonators present two different lengths  $l_1$  and  $l_2$  (associated to their resonance frequencies  $f_1$  and  $f_2$ ) for respectively resonators 1 and 2. Based on (10), and considering two loops, we can write the following equations:

$$- \begin{pmatrix} F_1 & F_2 \end{pmatrix} \begin{pmatrix} \alpha_1 & \frac{\gamma}{2} \\ \alpha_2 & \frac{\gamma}{2} \end{pmatrix} \begin{pmatrix} \Delta T \\ \Delta RH \end{pmatrix} = \begin{pmatrix} \Delta f_1 \\ \Delta f_2 \end{pmatrix} \quad (12)$$

where  $\Delta T = T - T_{ini}$ ,  $\Delta RH = RH - RH_{ini}$  with  $T_{ini}$  (respectively  $RH_{ini}$ ) the initial temperature (respectively relative humidity) at time  $t_0$ ,  $T$  (respectively  $RH$ ) the temperature (respectively relative humidity) at time  $t$  ( $t > t_0$ ).

The quantity  $F_n$  (independent of temperature and humidity) can be extracted using an initial measurement and (10). Indeed, by measuring the temperature  $T_{ini}$  and humidity  $RH_{ini}$  of the first measured resonance frequency  $f_{ini}^n$  of the resonator  $n$ , we have:

$$F_n = \frac{f_{ini}^n}{(1 - \alpha_n T_{ini} - \frac{1}{2}[a' + \gamma RH_{ini}])} \quad (13)$$

As the set of terms appearing in the second part of (13) is known, it is possible to calculate  $F_n$ . If the criterion  $\alpha_2 \neq \alpha_1$  is respected, (12) allows a unique expression for both temperature and humidity as follows :

$$\begin{cases} T = T_{ini} - \frac{1}{F_1 F_2 (\alpha_1 - \alpha_2)} (F_2 \Delta f_1 - F_1 \Delta f_2) \\ RH = RH_{ini} - \frac{2}{\gamma F_1 F_2 (\alpha_1 - \alpha_2)} [F_1 \alpha_1 \Delta f_2 - F_2 \alpha_2 \Delta f_1] \end{cases} \quad (14a) \quad (14b)$$

If the resonators are placed on the same substrate, they will present the same values for  $\gamma$  and  $a'$  and  $\alpha_p$  as well. However, even if scatterers are designed on the same substrate and the same metal for the resonator's pattern, the value of  $\alpha_c$  so  $\alpha$  varies with the resonator length (see [26]). Thus the fact of considering two different lengths means that we have  $\alpha_1$  not equal to  $\alpha_2$  in a vast majority of cases and especially in the case that will be presented next.

By doing a initial measurement of the resonance frequency  $f_{ini}^n$  for both resonators at a known temperature  $T_{ini}$  and humidity  $RH_{ini}$ , we can then calculate  $F_n$  using (13). To extract  $T$  and  $RH$  at time  $t$ , (14a) and (14b) will be applied on the measured resonance frequencies of the two resonators  $f_1$  and  $f_2$ . As previously said, coefficients  $\alpha$ ,  $\gamma$  and  $a'$  are

supposed to be known using (7), (8) and (9) for known tag materials and geometry or can either be obtained by measurement (see the procedure described in section VI). In the present paper, Rogers RO4003C will be used as a substrate. Note that its humidity dependence is not characterized by its provider. So, the procedure detailed in Section VI was first used to extract missing coefficients.

### B. Sensitivity of the measurement

The choice of the substrate which makes up the resonator is important for the accuracy of the sensor, especially for humidity. Temperature extraction is impacted by both the substrate and the metal part of the resonator [see (11)] while humidity can only be sensed by the substrate. More information related to this remark will be presented in Section III.

To increase the resolution of the sensor, the frequency resolution of the VNA has to be low. Indeed, the resonance frequency shift  $\Delta f$  due to temperature and humidity can be computed with [18]:

$$\Delta f = \frac{c}{2\sqrt{\varepsilon_{eff}}L} (\alpha \Delta T + \frac{1}{2} \gamma \Delta RH) \quad (15)$$

Using typical values for  $\alpha$  and  $\gamma$  (given later in the paper), we can find that an increase of 1°C leads to a frequency shift of 64kHz. The frequency step on the VNA during our measurements is 6kHz. Thus, the estimated temperature is discretized by steps of 1/11°C. Moreover, an error in the research of the curve maximum of only 11 frequency steps can lead to an error of 1°C. Therefore, increasing the number of frequency points during the measurement would reduce this error and this discretization.

Note that loop resonators are considered in this paper but other tag geometries can also be used. For example, in [18], (1) is also used for dipole over ground plane resonators. In this case, the expression of  $\alpha_p$  and also the transformation from  $\eta$  to  $\gamma$  is different and must be updated.

## III. SIMULATIONS

Prior to that, EM simulations using CST were achieved to make a proof of the sensor concept presented above. Figure 1 shows the tag, which is made up of two loop

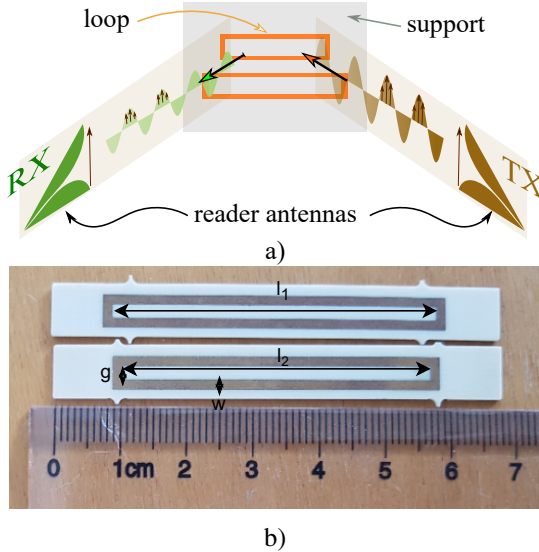


Fig. 1. a) Principle of the measurement of the scatterer's resonance frequency used to sense temperature and humidity. When the tag is placed in a climatic chamber, the temperature and humidity can be controlled in order to characterize the accuracy of the sensor function implemented. Real environment measurements are done in office-type environments. b) Resonators used for the measurements. The first resonator has  $g = 2$  mm,  $w = 1$  mm and  $l_1 = 49$  mm. The second resonator has the same  $g$  and  $w$  but  $l_2 = 46$  mm.

scatterers. For simulation, zinc and copper metals with corresponding thermal dilatations of  $\alpha_c^{copper} = 17 \times 10^{-6} \text{ }^\circ\text{C}^{-1}$  and  $\alpha_c^{zinc} = 31 \times 10^{-6} \text{ }^\circ\text{C}^{-1}$  are used.  $g = 2.07$  mm,  $w = 1.43$  mm, and  $l_1 = 47.97$  mm are the dimensions of the first copper resonator. The second zinc resonator has the same  $g$  and  $w$  values but a different length  $l_2 = 38.38$  mm. The permittivity of the simulated support is  $\epsilon_r(T, RH) = 3(1 + 40 \times 10^{-6} RH)(1 + 10 \times 10^{-6} T)$  where  $T$  and  $RH$  will fluctuate following  $0 < T < 60 \text{ }^\circ\text{C}$  and  $0 < RH < 100\%$ . The dielectric support is supposed linear with humidity so  $a = 0$ . A plane wave excitation and a Transient Solver are considered. The physical parameters used for the simulation are summarized in Table II. RCS simulation results are plotted in Fig. 2 for different temperature and humidities values. Equations (14a) and (14b) are then applied to the extracted resonance frequencies : 2.36 GHz and 2.91 GHz are the values obtained for the resonator 1 and 2 respectively.

Fig. 3a and b plot respectively the extracted temperature and relative humidity using (14a) and (14b) with the simulated resonance frequencies. The axes in Fig. 3 correspond to the temperature and humidity values imposed in the simulation. It can be seen that the extracted physical quantities are independent, which shows that the system of equations (12) can be solved.

The extracted temperature in Fig. 3a is in good agreement with the simulated temperature with an average error of  $2^\circ\text{C}$  (and a maximum of  $6^\circ\text{C}$ ). With humidity, a slightly larger error with  $3\%RH$  on average (and a maximum of  $9\%RH$ ) is observed.

A second simulation has been done where the previous parameters still apply except for the permittivity which is now described by  $\epsilon_r(T, RH) = 3.55(1 + 20 \times 10^{-6} RH)(1 +$

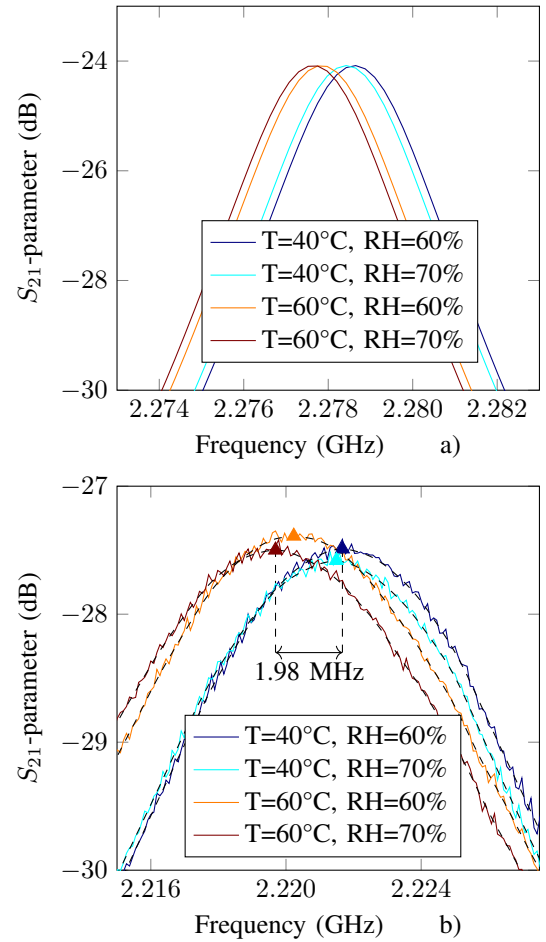


Fig. 2. a) Simulated RCS response of a resonator for different temperatures and humidities values. b) Smoothed measurement (dashed line) and raw data (continuous line) for  $S_{21}$  response at different temperature and humidity values. A gaussian smoothing using a moving window is used. The window is 200 frequency points width on a measurement of 10,001 points.

$40 \times 10^{-6} T)$ . The goal of this simulation is to demonstrate the concept discussed in Section II which is the importance of the substrate for the humidity extraction. The humidity dependence has been lowered compared to the value used in the previous simulation (a reduction of  $\eta$  from 40 to 20). For temperature,  $\beta$  was increased from 10 to 40. Extracted temperature and humidity are plotted in Fig. 4. The extracted temperature is in good agreement with the simulated temperature with a maximum error of  $4^\circ\text{C}$  and  $2^\circ\text{C}$  on average. For humidity, a maximum error of  $22\%RH$  and  $10\%RH$  on average are observed. We can confirm that by increasing the thermal dependence  $\beta$ , hence the frequency shift, it is easier to estimate the correct temperature. Meanwhile, by reducing the humidity dependence  $\eta$  and so its frequency shift, higher errors on the humidity extraction are observed. Also, we can see that the behaviour between the temperature and humidity is not symmetrical since a low value of  $10 \times 10^{-6}$  on  $\beta$  does not increase significantly errors compared to  $\eta$ . This behaviour appears since the temperature extraction is also impacted by the thermal dilatation of the resonator while humidity extraction is only impacted by the permittivity. Errors on the estimation for the four limits in temperature and humidity of

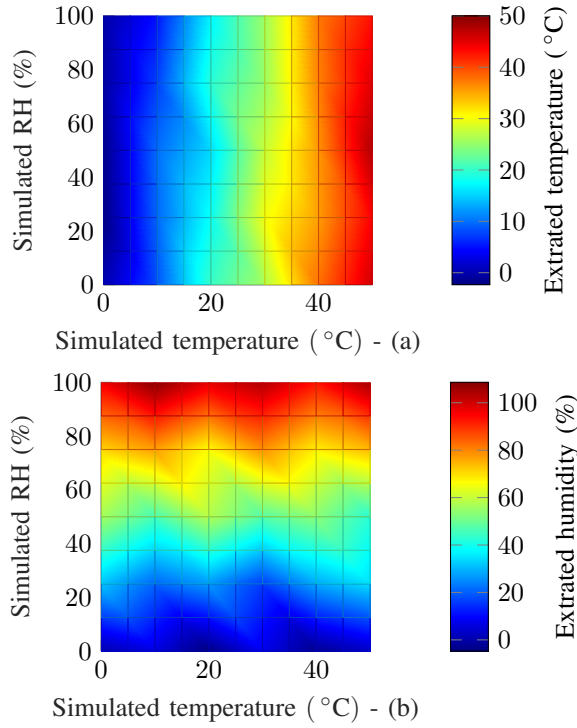


Fig. 3. a) Extrated temperature using (14a). b) Extrated relative humidity using (14b). The simulated chipless tag is shown in Fig. 1. The permittivity of the support is  $\epsilon_r = 3(1 + 40 \times 10^{-6}RH)(1 + 10 \times 10^{-6}T)$ .

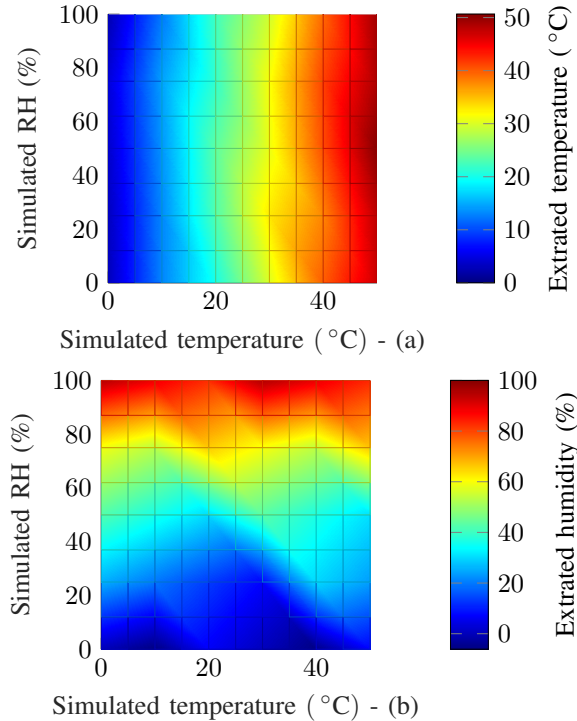


Fig. 4. a) Extrated temperature using (14a). b) Extrated relative humidity using (14b). The simulated chipless tag is shown in Fig. 1. The permittivity of the support is  $\epsilon_r = 3.55(1 + 20 \times 10^{-6}RH)(1 + 40 \times 10^{-6}T)$ .

the two simulations are listed in Table III and Table IV.

These simulations confirm the trends in extraction, but

TABLE II  
PHYSICAL PARAMETERS USED FOR THE SIMULATIONS.

Parameter	Simulation 1	Simulation 2
$\alpha_c^1$	$17 \times 10^{-6} \text{ }^\circ\text{C}^{-1}$	$17 \times 10^{-6} \text{ }^\circ\text{C}^{-1}$
$\alpha_c^2$	$31 \times 10^{-6} \text{ }^\circ\text{C}^{-1}$	$31 \times 10^{-6} \text{ }^\circ\text{C}^{-1}$
$\beta$	$10 \times 10^{-6} \text{ }^\circ\text{C}^{-1}$	$40 \times 10^{-6} \text{ }^\circ\text{C}^{-1}$
$\eta$	$40 \times 10^{-6} \text{ } \%\text{RH}^{-1}$	$20 \times 10^{-6} \text{ } \%\text{RH}^{-1}$
$\epsilon_r$	3	3.55
$g_1$	2.07 mm	2.07 mm
$g_2$	2.07 mm	2.07 mm
$w_1$	1.43 mm	1.43 mm
$w_2$	1.43 mm	1.43 mm
$l_1$	47.97 mm	47.97 mm
$l_2$	38.38 mm	38.38 mm

TABLE III  
ESTIMATION ERROR IN SIMULATION FOR FIG. 3.

	Temperature (°C)	Humidity (%RH)
T=0°C, RH=0%RH	0	0
T=0°C, RH=100%RH	0.5	3.7
T=50°C, RH=0%RH	3.8	2.9
T=50°C, RH=100%RH	7	5

TABLE IV  
ESTIMATION ERROR IN SIMULATION FOR FIG. 4.

	Temperature (°C)	Humidity (%RH)
T=0°C, RH=0%RH	3	0
T=0°C, RH=100%RH	2.4	5
T=50°C, RH=0%RH	2.8	7
T=50°C, RH=100%RH	0.7	17

they do not allow to estimate very precisely the error to be expected when using (14a). Indeed, despite a very dense mesh, and therefore a very long simulation time, the numerical accuracy obtained in the simulation remains relatively low and induces significant errors which will not be present in measurement. It is the experimental study that will allow us to better characterise the errors obtained on the extraction of temperature and humidity.

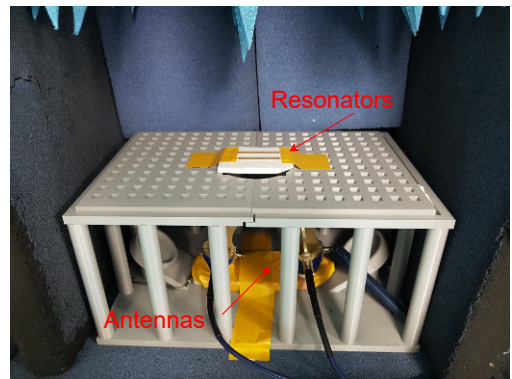


Fig. 5. Photo of the measurement bench and tags inside the climatic chamber.



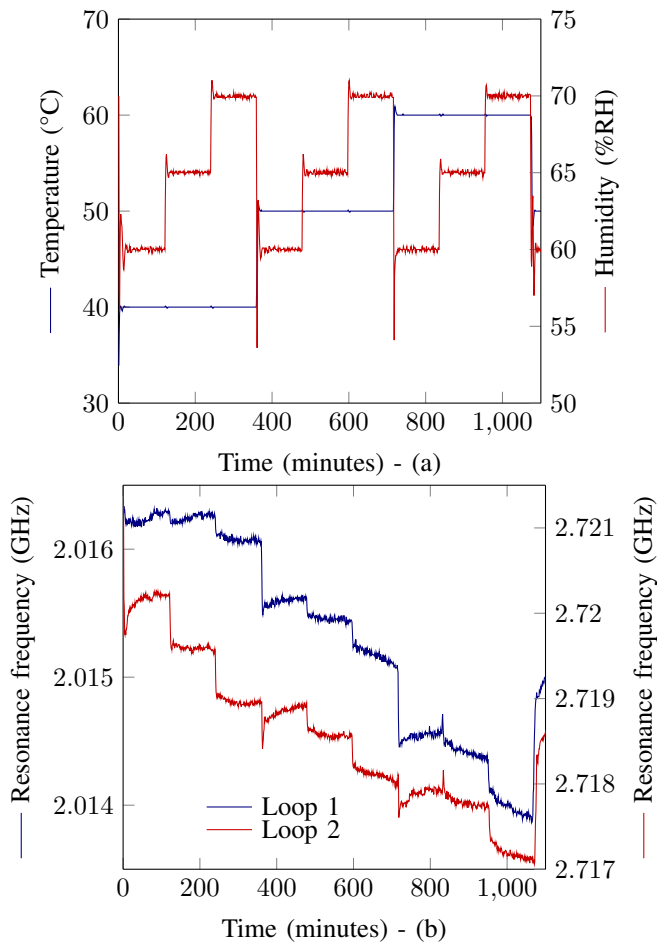


Fig. 6. a) Temperature and humidity measured inside the climatic chamber by an electronic sensor as a function of time. b) Measurement of the resonance frequency of the two resonators as a function of time.

#### IV. SENSING IN A CONTROLLED ENVIRONMENT

The introduced approach is mainly based on the measurement of scatterer resonance frequencies. This information can be obtained from the measurement of the RCS of the scatterer [28], a quantity that can be easily obtained in simulation. In practice, it is not necessary to have the RCS, the measurement of the  $S_{21}$  parameter in bi-static configuration and in frequency is sufficient. Indeed, the resonance frequencies are intrinsic to the scatterers and do not depend on the measurement setup like the distance between the antennas and the tag or the antennas themselves [29].

##### A. Measurement setup and tag design

Fig. 5 presents the measurement setup and the fabricated tags used are shown Fig. 1. Experimental measurements are performed using a VNA (Agilent 5222A). The source power of VNA is equal to 0 dBm. The frequency sweep ranging from 2 to 3 GHz with 10001 points is used. A co-polarization bi-static configuration with Satimo (QH2000) quad ridged open boundary antennas (2–32 GHz) is used.

Temperature and humidity are controlled using a Votsch climatic chamber VC0018. To lower the level of reflection,

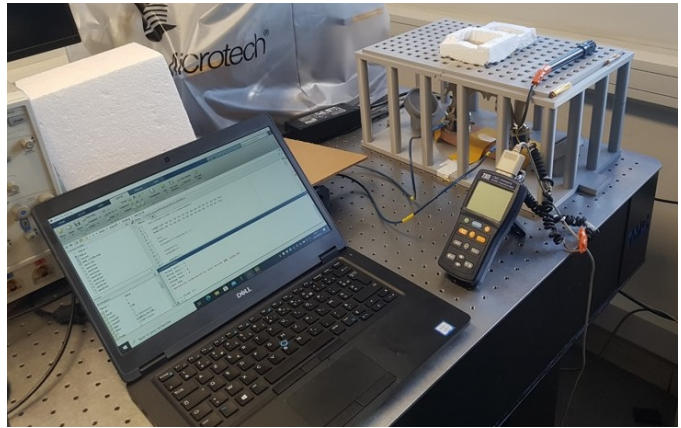


Fig. 7. Photo of the measurement bench and tags.

absorbers are installed inside the chamber (see Fig. 5). To improve isolation, a bistatic antenna arrangement is used. The following technique is followed for the measurements: initially, the temperature in the climatic chamber is set. The  $S_{21}$  parameter is measured with a VNA once the temperature is stabilized. An electronic sensor measures the temperature and humidity inside the chamber. The measured S-parameters have been smoothed to reduce any remaining measurement noise that could affect the resonance frequency search (peak apex detection) and consequently cause a frequency extraction error. During the VNA experiments, an IF bandwidth of 10kHz was also used.

In practice, a standard PCB chipless tag was measured. On a Rogers RO4003C substrate, the tag is made up of two copper resonators (see Fig. 1b). By using different resonator lengths, the requirement  $\alpha_1 \neq \alpha_2$  is respected (see [26, eq. (5)]). The humidity dependency for this substrate is not indicated by the provider. As a result, we have extracted the values of  $\gamma$  and  $a'$  first. The method to identify these parameters is presented in Section VI. A variation of temperature from 40°C to 60°C with a 10°C step is achieved as well as a variation of the relative humidity from 60%RH to 70%RH with 5%RH steps. The temperature and humidity profiles are shown in red in Fig. 6a. Both resonators are placed at the same time side by side (as shown in Fig. 5) for the measurement and were not moved during the whole monitoring.

##### B. Results and Analysis

The measured resonance frequencies are plotted in Fig. 6b. Variations of 20°C and 20%RH are achieved and (14a) and (14b) are applied. The results of the extraction are shown in Fig. 8 alongside the temperature and humidity measured by the electronic sensor.

The highest difference with the electronic temperature sensor is of 2.8°C and 0.95°C on average. For humidity, the highest difference is very localized near 700min and equals to 7.2%RH. On average, an error of 2.1%RH was made with the electronic sensor. We can see that humidity is estimated with more errors than temperature. Indeed, as presented in section III, the humidity impact tends to be lower than the temperature one since it is only sensed by one physical mechanism (the

substrate variation) and so induces smaller shifts which are harder to measure. This is the case for copper resonators on Rogers RO4003C. Investigations on substrate properties will be presented later in section VI and Table V.

## V. SENSING IN A REAL ENVIRONMENT

### A. Measurements

Measurements were done in a real environment to validate the sensing approach. The measurement setup is shown in Fig. 7 and the tags used in practice are presented in Fig. 1. The bistatic antenna configuration is kept to increase the isolation. A computer is connected to a VNA and an electronic temperature and humidity sensor. Each minute, the computer triggers measurements on the VNA and the sensor. Temperature, humidity and the S-parameters are saved on the computer. The measured S-parameters have been smoothed to remove any residual measurement noise that may impact the search of the resonance frequency and thus induce an error on the frequency extraction. The tag was not moved during the whole monitoring.

### B. Results and analysis

The recorded temperature and humidity during the measurement are shown in Fig. 9 in red. The measurement lasted 2200 minutes. Equations (14a) and (14b) are applied and the estimated temperature and humidity are shown in Fig. 9 in blue alongside the electronic sensor in red. We can see that the two quantities are in good agreement with an error lower than  $1^{\circ}\text{C}$  and  $5\%RH$  on the estimated quantities. In Fig. 9 the estimated temperature which can be sensed using a traditional chipless RFID temperature sensor is also plotted in brown. As said in the introduction, if the humidity effect is not considered, a higher error of  $2^{\circ}\text{C}$  on the extracted temperature can be observed. The  $2^{\circ}\text{C}$  error is obtained for relatively low humidity values (around  $30\%$ ), and would be even greater if humidity increases. This approach shows how it is possible with (14a) to reduce the errors in the estimation of temperature as well as enabling to sense more physical quantities (here humidity).

## VI. DISCUSSIONS ON THE PROPOSED APPROACH

### A. Discussion on measurement conditions

The introduced tags allow to perform an identification and a sensor function (temperature, humidity) simultaneously. It should be noted that the measurement conditions associated with these two functions are quite different from each other. Indeed, for the identification function, the objective in application is to be able to retrieve information in the most constrained environments, potentially in motion, and an interesting example to illustrate this type of measurement condition is when the tag is held in the hand. To this end, several approaches have been introduced to make the measurement as independent as possible of the environment, even if the tag is coupled with the unknown object on which it is placed [30], [31]. The measurement in connection with the sensor functionality is quite different and requires to further constrain the measurement conditions [18], [26]. This also means that

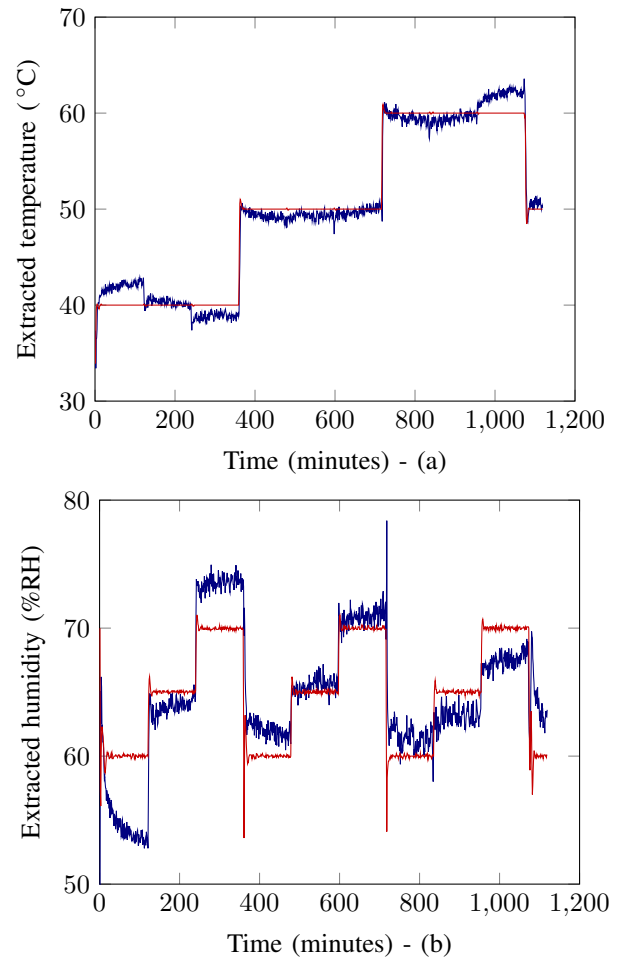


Fig. 8. a) Extracted temperature in blue using (14a) and measured temperature with the electronic sensor in red. b) Extracted relative humidity using (14b) in blue and measured with the electronic sensor in red. The test-bench is shown in Fig. 5.

it will always be possible to obtain the tag identifier when reading in sensing mode, whereas the reverse is not true. In identification, we can allow a margin of  $80\text{ MHz}$  on the detection of the resonant frequency for the decoding of the information, in sensor, we will try to measure the smallest variations of the resonance frequency and we must therefore make sure that this variation is linked to the physical parameters that we are measuring and not to the changing environment. As an example, a variation of  $0.8\text{ MHz}$  (i.e. 100 times less than for the identification mode) is equivalent to a change of  $6^{\circ}\text{C}$  in temperature for the tags presented. Therefore, the results presented in sections IV and V are only possible if the environment (excluding temperature and humidity variations) and the measurement system have an effect on the resonant frequency of less than  $0.1\text{ MHz}$  ( $64\text{ kHz}$  for  $1^{\circ}\text{C}$  of error as discussed in the last part of section II). To illustrate that, it is important to note that in an environment where nothing moves in the vicinity of the tag (i.e. within a radius of one meter centered on the reading zone), the action of taking the tag and replacing it strictly in the same place implies a modification of the resonance frequency of around  $0.8\text{ MHz}$ . This figure shows that 1) the error due to the environment on the tag's



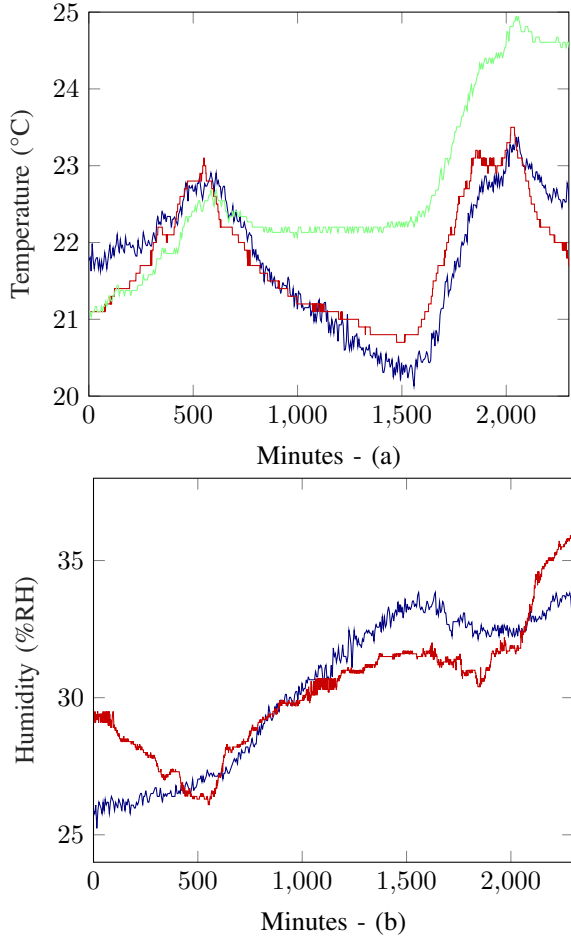


Fig. 9. a) Extracted temperature in blue using (14a), measured temperature with the electronic sensor in red and temperature sensing only in green. b) Extracted relative humidity using (14b) in blue and measured with the electronic sensor in red. The test-bench is shown in Fig. 7.

resonance frequency can be reduced very significantly when the environment is perfectly stationary, 2) any displacement of the tag, even if very small, leads to significant errors for the sensor function. This is why the measurement conditions implemented in the article impose a fixed environment around the tag and a fixed tag that is not moved during the measurement [18]. The person carrying out the measurements stands at a distance of at least one meter from the tag and most of the measurements are carried out without any person in the room where the experiment takes place. In terms of measurement methodology, the principle of extraction is based on 1) the initial measurement of the resonance frequency (at time  $t_0$ ) as well as the temperature and humidity, 2) successive measurements at time  $t$  of the resonance frequency under the same conditions as the measurement at  $t_0$  where only the humidity and temperature vary over time. The difference in resonance frequency  $\Delta f = f(t) - f(t_0)$  obtained thus contains information on the effects of the variation of the physical parameters on the resonator, effects which are modeled and given by (12). Note that the fact of imposing not to move the tag or the environment in contact to the tag during the measurement is not incompatible with applications, we can

give the example of a sensor fixed in a building and positioned far from human activities. Under these conditions, temperature and humidity can be extracted remotely with simple resonators manufactured with classical PCB manufacturing techniques. Note also that we do not use any specific materials that are particularly sensitive to humidity or temperature for the sensor function (the RO substrate is known to be relatively insensitive to humidity variations). Also, depending on the application, it is always possible to select another substrate to reduce the reading constraints specified here.

### B. Parameters characterization

Substrate temperature variations are often given by providers in the data sheet but humidity response is often not characterized. This section will show how to characterize the coefficients  $a'$ ,  $\alpha$  and  $\gamma$  with an example of Rogers RO4003C substrate. The time transient response as well as the limiting range of (10) will also be studied for this dielectric.

By normalizing the measured resonance frequency  $f$  in (10) by (13), we have :

$$\frac{f}{F} = 1 - \frac{a'}{2} - \alpha T - \frac{\gamma}{2} RH \quad (16)$$

By considering  $f_{ini}$  as the first measured resonance frequency at time  $t_0$ , as the coefficients  $a'$ ,  $\alpha$ ,  $\gamma$  are small compared to one (see Table V), one can simplify (13). From this, we can rewrite (16) as follows. Note that this simplifying assumption will be validated later.

$$\frac{f}{f_{ini}} \simeq 1 - \frac{a'}{2} - \alpha T - \frac{\gamma}{2} RH \quad (17)$$

From (17) it is possible to extract the coefficients  $a'$ ,  $\alpha$  and  $\gamma$  by linear regression applied on measurement. Indeed, it is possible to have the resonance frequencies corresponding to a set of different values of temperature and humidity. The set of measurements presented in section IV, as long as we have measured at the same time the temperature and the humidity with an independent electronic sensor can be used to make this extraction.

Measurements in the climatic chamber with temperature and humidity profiles such as the one shown in Fig. 10-a have been used to extract the three coefficients. Indeed, once the frequencies  $f$  were measured alongside the temperature  $T$  and humidity  $RH$ , a fit of all the realized measurements was done based on (17) to find the values of  $\alpha_n$ ,  $\gamma$  and  $a'$  and is illustrated in Fig. 10-b. This extraction was repeated three times. For each measurement, the entire test bench was disassembled and put back in place. Extracted coefficients are listed in Table V. The measurement in a real environment of Section V is also used to estimate these coefficients and the obtained results are added in Table V. Fig. 11 shows a comparison between the normalized resonance frequency and (17) using the measurements obtained in real environment. We can see that the fitting is in good agreement for different humidity and temperature variations.

We can see that the extracted coefficients in the climatic chamber (for a sensing range of 40°C-60°C and 60%RH-70%RH) are very close to each other, reflecting a good

TABLE V  
FITTING COEFFICIENTS OF (17) FOR DIFFERENT MEASUREMENTS USING  
THE SAME RESONATOR.

	Measure 1	Measure 2	Measure 3	Real environment
$\alpha$	$3.852 \times 10^{-5}$	$4.624 \times 10^{-5}$	$4.165 \times 10^{-5}$	$4.131 \times 10^{-5}$
$\gamma$	$2.658 \times 10^{-5}$	$3.108 \times 10^{-5}$	$2.926 \times 10^{-5}$	$2.836 \times 10^{-5}$
$a'$	0.004	0.006	0.006	0.004

repeatability of the measurement. In comparison to the real environment estimation, we can see that the setup has a limited impact on the extraction. Also, in the real environment the measurement was done in the range of 20°C-25°C and 25%RH-40%RH as shown in Fig. 9. It means that the linear approximation of humidity made for the Rogers RO4003C (which is uncharacterized in terms of humidity) seems a good approximation for the whole 25%RH-70%RH range. This range of validity for our substrate and the limits of the approach will be discussed later in section VI. D.

Some of the extractions presented here were also done using the same approach (linear regression on a set of measurements made at different times for different values of temperature and humidity) applied on (16), i.e. before the simplification indicated above. The results obtained are close to those presented in Table IV, with an error of less than 10% on each coefficient. This value of 10% will be taken into consideration in subsection E. to calculate the uncertainty and the error induced on the extraction of temperature and humidity. However, the extraction from (16) is more difficult to implement. Indeed, it has been seen in practice that this extraction is strongly dependent of the initial values given to  $a'$ ,  $\alpha$  and  $\gamma$  since  $F$  also depends on these parameters as stated in (13). This is not the case with (17) where the obtained results are independent from the initial values given to these coefficients. This is the reason why only the extracted values obtained with (17) are used in this paper.

### C. Time transient responses

The measurement done to identify the parameters in the climatic chamber in Fig. 10 permits to find the same coefficients as the ones obtained with the measurement in a real environment. We also note that the measurement in the climatic chamber offers additional information on the time response of the sensor. Indeed, since we can change temperature and humidity more quickly in the climatic chamber, we can see in Fig. 10 the transient response of the sensor, i.e. the time response of the Rogers RO4003C substrate in regard to humidity variations. According to the estimated humidity in the previous section, as well as the comparison with the real environment fitting where this time response was not taken into account, we can neglect this effect for this particular substrate. Indeed, fitting the measured frequency to (17) using the end of humidity steps only (where the transient time is nearly over), leads to  $\alpha = 4.190 \times 10^{-5} \text{C}^{-1}$  and  $\gamma = 3.710 \times 10^{-5} \% \text{RH}^{-1}$  instead of  $\alpha = 4.165 \times 10^{-5} \text{C}^{-1}$  and  $\gamma = 2.934 \times 10^{-5} \% \text{RH}^{-1}$  when considering the whole response. This measurement correspond to measure n°3 in

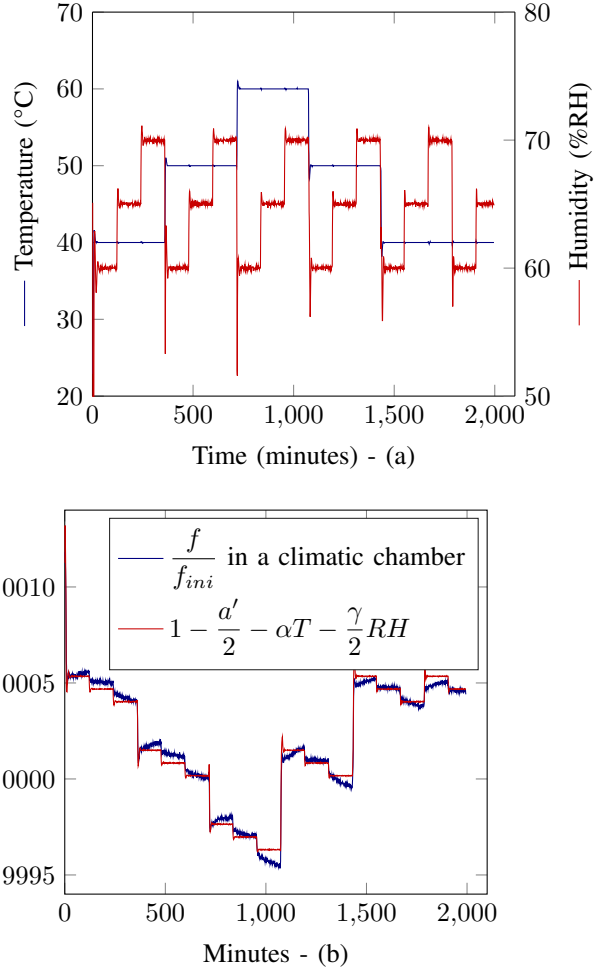


Fig. 10. a) Temperature and humidity measured with an electronic sensor. b) Measured normalized resonance frequency in a climatic chamber in blue and (17) using estimated parameters in red with  $\alpha = 4.165 \times 10^{-5} \text{C}^{-1}$  and  $\gamma = 2.926 \times 10^{-5} \% \text{RH}^{-1}$  (see Table V).

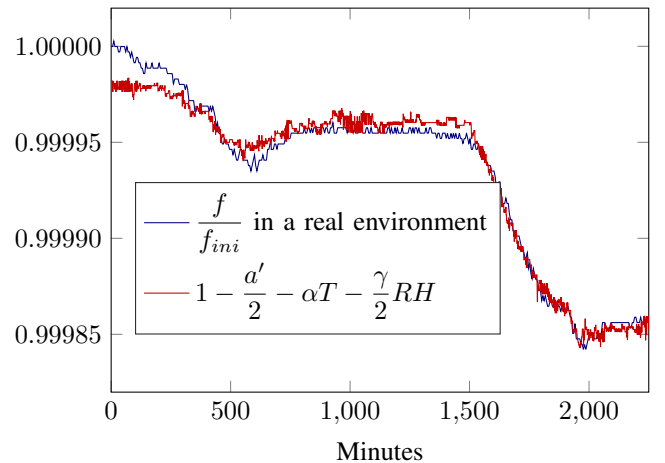


Fig. 11. Measured normalized resonance frequency in a real environment in blue and (17) using estimated parameters in red with  $\alpha = 4.131 \times 10^{-5} \text{C}^{-1}$ ,  $\gamma = 2.836 \times 10^{-5} \% \text{RH}^{-1}$  and  $a' = 0.004$  (see Table V). Temperature and humidity variations of this measurement are presented in Fig. 9.

Table V. For measurements every minute, we can notice that the impact on temperature response time is negligible and the

TABLE VI  
FITTING COEFFICIENT  $\gamma$  OF (17) FOR DIFFERENT HUMIDITY RANGE.

	Relative humidity range	Estimated $\gamma$ by fitting
Measure n°1	25-40 %	$2.836 \times 10^{-5} \%RH^{-1}$
Measure n°2	60-70 %	$2.926 \times 10^{-5} \%RH^{-1}$
Measure n°3	60-70 %	$2.934 \times 10^{-5} \%RH^{-1}$
Measure n°3	70-75 %	$2.876 \times 10^{-5} \%RH^{-1}$
Measure n°3	75-80 %	$2.808 \times 10^{-5} \%RH^{-1}$
Measure n°3	80-85 %	$7.524 \times 10^{-5} \%RH^{-1}$
Measure n°3	85-90 %	$13.754 \times 10^{-5} \%RH^{-1}$
Measure n°3	90-95 %	$33.5 \times 10^{-5} \%RH^{-1}$

impact on humidity is low confirming the results previously presented.

#### D. Parameters limitations

Unlike temperature dependence of the permittivity, which can often be considered linear for classical materials used for tag fabrication in a range that could be around 0-100 °C, the linearization of humidity dependence in (3) is only valid for a limited range of humidity around a specific value. However, to increase this range of definition, it is possible to use a model with more parameters [compared to (3)] describing a nonlinear variation of the permittivity with humidity. This model can be based on a polynomial fitting of order 2 or 3 for example.

Furthermore, some materials such as Kapton dielectrics, have been characterized in both humidity and temperature variations [32]. The thermal and humidity dependencies are linear and are valid on 0°C-200°C and 0%RH-100%RH ranges. With similar materials, the linear assumption is valid for the whole 0-100 %RH sensing range. In reality, close to 100 %RH, the presented approach will not work since water droplets will start to form on the surface of the tag. The presence of water will heavily impact the resonance frequency of the resonator due to its high permittivity ( $\epsilon_{\text{water}} \simeq 80$ ). Measurements with different humidity values have been done in order to determine this limitation for the dielectric used in this paper (Rogers RO4003C). An example of normalized resonance frequency used to extract the coefficient  $\gamma$  is plotted in Fig. 12. The estimated  $\gamma$  for different humidity ranges are presented in Table VI. The 25%RH-40%RH range was the one considered during the measurement in a real environment. The last measurement (measurement n°3) was done from 60%RH to 95%RH and divided in sub-domains. Between these measurements, the test-bench was completely disassembled and put back together. We can see that  $\gamma$  is quite constant for humidity values lower than 75 %RH. For higher values,  $\gamma$  significantly increases with the humidity and the linear model cannot be used to extract the relative humidity on the total humidity range considered here. At 85 %RH, the value of  $\gamma = 2.8 \times 10^{-5} \%RH^{-1}$  does not describe well the humidity dependence of the resonator and so can be considered as a limitation of (10) here this linear approximation model is considered on this wide range. In Fig. 13 are plotted the extracted humidity values using a value of  $\gamma_{25-80} = 2.8 \times 10^{-5} \%RH^{-1}$ , which corresponds to the 25-80 %RH extraction range and a value of  $\gamma_{90-95} = 33.5 \times 10^{-5} \%RH^{-1}$ , which corresponds

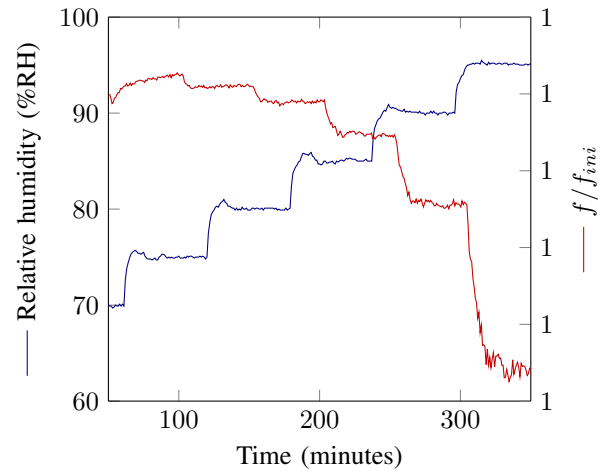


Fig. 12. a) Measured humidity with an electronic sensor in the climatic chamber with a constant temperature of 40°C. b) Normalized resonance frequency  $f/f_{ini}$  for the different humidity values used to extract  $\gamma$ .

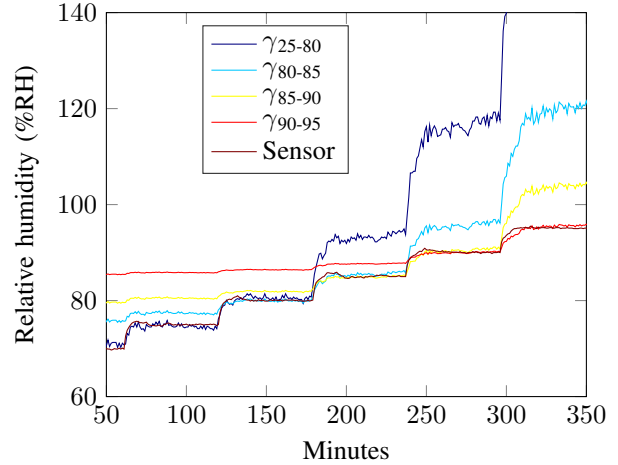


Fig. 13. Extracted humidity using different  $\gamma$  compared with the real humidity measured with a reference sensor (noted sensor in the figure) for a constant temperature of 40°C.

to the 90-95 %RH extraction range. We can see that using a constant  $\gamma_{25-80}$  for the linear approximation allows a good extraction until 80 %RH but does not describe well a higher humidity range. At the same time,  $\gamma_{90-95}$  only permits to have the correct value in the 90-95 %RH range with 10 %RH error for a real humidity of 70 %RH.

#### E. Monte Carlo simulations

Monte Carlo simulations have been made to estimate the error done on the estimation of the humidity and temperature as well as uncertainties. The RCS curves of Fig. 2 have been used with a SNR of 40dB which is a coherent value measured in practice. Resonators were chosen to have  $f_1 = 3\text{GHz}$ ,  $\alpha_1 = 16 \times 10^{-6} \text{C}^{-1}$ ,  $f_2 = 3.2\text{GHz}$ ,  $\alpha_2 = 32 \times 10^{-6} \text{C}^{-1}$  and  $\gamma = 40 \times 10^{-6} \%RH^{-1}$ . Monte-Carlo simulations show no particular behavior which means that the estimation is without bias (not shown here). Errors are quite low with less than 1°C on the temperature and less than 0.5% on

the humidity. Uncertainties are  $2.6^{\circ}\text{C}$  for temperature and  $1.5\%$  for humidity. To increase the temperature and humidity accuracy and sensibility, dielectrics with higher temperature and humidity dependencies (like Kapton [32]) as well as a resonator made of metals with higher dilatation coefficients (like zinc) should be used. By doing so, coefficients  $\alpha_1$  and  $\alpha_2$  in (10) will increase, resulting in higher frequency shifts which are easier to measure. Also, by looking at (14a) or using (14b), one can notice that the temperature and humidity resolution are immediately linked to the frequency steps used for the measurements. Hence having a lower frequency step increases the resolution of the measurands.

Uncertainties on the parameters  $\alpha$  and  $\gamma$  in (14a) and (14b) can also impact the estimation, so we also studied the errors and uncertainties resulting from an error on these parameters. Results are plotted in Fig. 14 and Fig. 15. We can see that the errors and uncertainties introduced on the extracted temperature and humidity are higher than the ones coming from an error from the measurement of the resonance frequency. We can also notice a tendency in which the uncertainty increases for the estimated temperature as temperature increases and the uncertainty for the estimated humidity increases when temperature or humidity increase.

It is notable that (14a) does not depend on  $\gamma$  and so the error on the estimated temperature only increases as  $T$  increases. Meanwhile, (14b) does depend on both  $\alpha$  and  $\gamma$  and so the error increases as  $T$  or  $RH$  increases.

Overall, even with high uncertainty, the sensor functionality remains possible as demonstrated in the measurements. Indeed, a high uncertainty means that the estimated quantities are in an interval of  $\pm 10\%RH$  for humidity as an example for  $\Delta T = 80^{\circ}\text{C}$  and  $\Delta RH = 80\%$ . But the error stays low for both estimated quantities so on average, the estimated quantities are close to the real quantities. This average is easy to do on a measurement by using the average functionality of the VNA.

It is reminded that the sensitivity of the measurement is directly related to the accuracy of the measuring device. The use of a VNA is perfectly suitable with a high dynamic of measurement and the resolution in frequency essential to implement the introduced approach.

## VII. CONCLUSION

A combined temperature and humidity sensor for RFID chipless applications is described in this paper. This functionality can be added to current frequency chipless RFID tags at no additional expense while maintaining their identification capabilities. Indeed, such small shifts in the resonance frequency do not impact the chipless RFID identification scheme. It is shown that two physical quantities such as temperature and humidity can be extracted independently using only the measurement of resonance frequencies of resonators positioned on a label and interrogated remotely using a radar approach. We also note that these two quantities are obtained simultaneously and that the tags used do not include any specific materials which makes them very accessible. Simulation and real-life measurements are used to validate the sensor model. The linear approach for

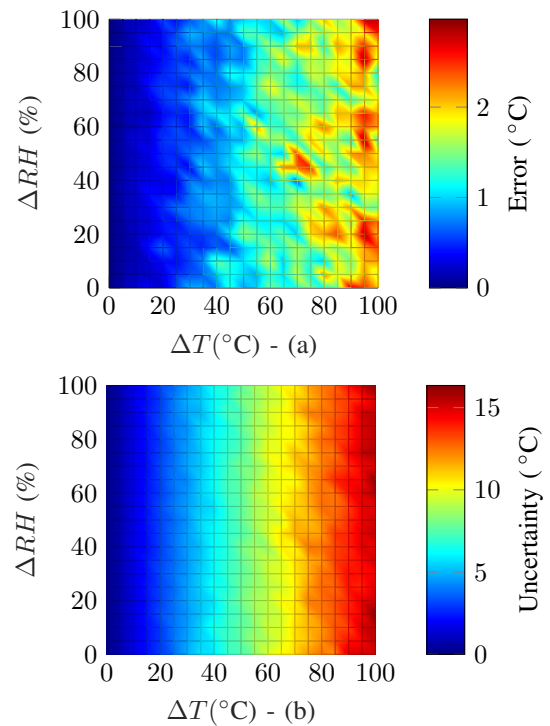


Fig. 14. a) Errors and b) uncertainties on the estimated temperature as a function of real values of temperature and humidity with an uncertainty of 10% on  $\alpha, \gamma$ .

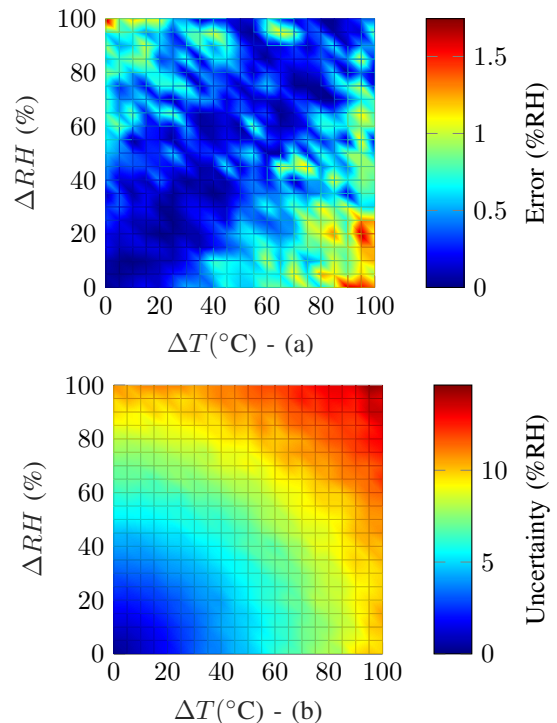


Fig. 15. a) Errors and b) uncertainties on the estimated humidity as a function of real values of temperature and humidity with an uncertainty of 10% on  $\alpha, \gamma$ .

a Rogers RO4003C substrate was determined to work up to  $80\%RH$  with errors of  $1^{\circ}\text{C}$  and  $5\%RH$  in the real environment and  $1^{\circ}\text{C}$  and  $2\%RH$  in an anechoic climatic chamber. Example



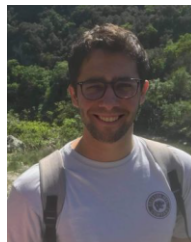
application scenarios can be found in the monitoring of human beings in building or the monitoring of the cold chain in the food industry. In the case of more severe environments, a packaging specifically designed for the tag, would make it possible to avoid certain irremediable deteriorations like corrosion (of the metal or the substrate).

#### ACKNOWLEDGMENT

This project has received funding from the European Research Council (ERC) under the European Union's Horizon 2020 research and innovation program (grant agreement No 772539). This work is also supported by Univ. Grenoble Alpes. The authors are also thankful towards Nathalie Franck for her help in proofreading the paper.

#### REFERENCES

- [1] J. Landt, "The history of RFID," *IEEE Potentials*, vol. 24, no. 4, pp. 8–11, 2005.
- [2] S. Preradovic and N. C. Karmakar, "Chipless RFID: Bar code of the future," *IEEE Microw. Mag.*, vol. 11, no. 7, pp. 87–97, 2010.
- [3] A. Vena, E. Perret, and S. Tedjini, "High-capacity chipless RFID tag insensitive to the polarization," *IEEE Trans. Antennas Propag.*, vol. 60, no. 10, pp. 4509–4515, 2012.
- [4] C. Herrojo, M. Moras, F. Paredes, A. Núñez, E. Ramon, J. Mata-Contreras, and F. Martín, "Very low-cost 80-bit chipless-RFID tags inkjet printed on ordinary paper," *Technologies*, vol. 6, no. 2, p. 52, 2018.
- [5] C. Herrojo, M. Moras, F. Paredes, A. Nunez, J. Mata-Contreras, E. Ramon, and F. Martin, "Time-domain-signature chipless RFID tags: Near-field chipless-RFID systems with high data capacity," *IEEE Microw. Mag.*, vol. 20, no. 12, pp. 87–101, 2019.
- [6] M. Polivka, J. Havlicek, M. Svanda, and J. Machac, "Improvement in robustness and recognizability of RCS response of U-shaped strip-based chipless RFID tags," *IEEE Antennas Wireless Propag. Lett.*, vol. 15, pp. 2000–2003, 2016.
- [7] N. Barbot, O. Rance, and E. Perret, "Chipless RFID reading method insensitive to tag orientation," *IEEE Trans. Antennas Propag.*, 2020.
- [8] R. Nair, M. Barahona, D. Betancourt, G. Schmidt, M. Bellmann, D. Höft, D. Plette-meier, A. Hübler, and F. Ellinger, "A fully printed passive chipless RFID tag for low-cost mass production," in *The 8th European Conference on Antennas and Propagation*, 2014, pp. 2950–2954.
- [9] A. Guillet, A. Vena, E. Perret, and S. Tedjini, "Design of a chipless RFID sensor for water level detection," in *International Symposium on Antenna Technology and Applied Electromagnetics*, 2012, pp. 1–4.
- [10] J. Zhou and J. Shi, "RFID localization algorithms and applications—a review," *Journal of intelligent manufacturing*, vol. 20, no. 6, p. 695, 2009.
- [11] S. Shrestha, M. Balachandran, M. Agarwal, V. V. Phoha, and K. Varahramyan, "A chipless RFID sensor system for cyber centric monitoring applications," *IEEE Trans. Microw. Theory Tech.*, vol. 57, no. 5, pp. 1303–1309, 2009.
- [12] E. M. Amin, M. S. Bhuiyan, N. C. Karmakar, and B. Winther-Jensen, "Development of a low cost printable chipless RFID humidity sensor," *IEEE Sensors J.*, vol. 14, no. 1, pp. 140–149, 2013.
- [13] M. Borgese, F. A. Dicandia, F. Costa, S. Genovesi, and G. Manara, "An inkjet printed chipless RFID sensor for wireless humidity monitoring," *IEEE Sensors J.*, vol. 17, no. 15, pp. 4699–4707, 2017.
- [14] S. Fan, T. Chang, X. Liu, Y. Fan, and M. M. Tentzeris, "A depolarizing chipless RFID tag with humidity sensing capability," in *IEEE International Symposium on Antennas and Propagation*, 2018, pp. 2469–2470.
- [15] E. M. Amin and N. Karmakar, "Development of a chipless RFID temperature sensor using cascaded spiral resonators," in *SENSORS*, 2011, pp. 554–557.
- [16] J. Virtanen, L. Ukkonen, T. Björninen, L. Sydänheimo, and A. Z. Elsherbeni, "Temperature sensor tag for passive UHF RFID systems," in *IEEE Sensors Applications Symposium*, 2011, pp. 312–317.
- [17] T. Noor, A. Habib, Y. Amin, J. Loo, and H. Tenhunen, "High-density chipless RFID tag for temperature sensing," *Electronics Letters*, vol. 52, no. 8, pp. 620–622, 2016.
- [18] F. Requena, M. Gilch, N. Barbot, D. Kaddour, R. Siragusa, F. Costa, S. Genovesi, and E. Perret, "Thermal modeling of resonant scatterers and reflectometry approach for remote temperature sensing," *IEEE Trans. Microw. Theory Tech.*, 2021.
- [19] F. Requena, N. Barbot, D. Kaddour, and E. Perret, "Chipless RFID temperature and humidity sensing," in *IEEE MTT-S International Microwave Symposium*, pp. 545–548, 2021.
- [20] A. Vena, L. Sydänheimo, M. M. Tentzeris, and L. Ukkonen, "A fully inkjet-printed wireless and chipless sensor for CO<sub>2</sub> and temperature detection," *IEEE Sensors Journal*, vol. 15, no. 1, pp. 89–99, 2014.
- [21] T. T. Thai, F. Chebila, J. M. Mehdi, P. Pons, H. Aubert, G. R. DeJean, M. M. Tentzeris, and R. Plana, "Design and development of a millimetre-wave novel passive ultrasensitive temperature transducer for remote sensing and identification," in *The 40th European Microwave Conference*. IEEE, 2010, pp. 45–48.
- [22] B. Kubina, M. Schüßler, C. Mandel, A. Mehmood, and R. Jakob, "Wireless high-temperature sensing with a chipless tag based on a dielectric resonator antenna," in *SENSORS, 2013 IEEE*. IEEE, 2013, pp. 1–4.
- [23] J. G. Hester and M. M. Tentzeris, "Inkjet-printed flexible mm-wave van-atta reflectarrays: A solution for ultralong-range dense multitag and multisensing chipless rfid implementations for iot smart skins," *IEEE Transactions on Microwave Theory and Techniques*, vol. 64, no. 12, pp. 4763–4773, 2016.
- [24] A. Vena, E. Perret, D. Kaddour, and T. Baron, "Toward a reliable chipless rfid humidity sensor tag based on silicon nanowires," *IEEE Transactions on Microwave Theory and Techniques*, vol. 64, no. 9, pp. 2977–2985, 2016.
- [25] O. Rance, R. Siragusa, P. Lemaître-Auger, and E. Perret, "Contactless characterization of coplanar stripline discontinuities by RCS measurement," *IEEE Trans. Antennas Propag.*, vol. 65, no. 1, pp. 251–257, 2016.
- [26] F. Requena, N. Barbot, D. Kaddour, and E. Perret, "Contactless characterization of metals thermal expansion coefficient by a free-space RF measurement," *IEEE Trans. Antennas Propag.*, vol. 69, no. 2, pp. 1230–1234, 2020.
- [27] E. Chen and S. Y. Chou, "Characteristics of coplanar transmission lines on multilayer substrates: Modeling and experiments," *IEEE Trans. Microw. Theory Tech.*, vol. 45, no. 6, pp. 939–945, 1997.
- [28] A. Vena, E. Perret, and S. Tedjini, "Chipless rfid tag using hybrid coding technique," *IEEE Transactions on Microwave Theory and Techniques*, vol. 59, no. 12, pp. 3356–3364, 2011.
- [29] Z. Ali, E. Perret, N. Barbot, and R. Siragusa, "Extraction of aspect-independent parameters using spectrogram method for chipless frequency-coded rfid," *IEEE Sensors Journal*, vol. 21, no. 5, pp. 6530–6542, 2020.
- [30] A. Vena, E. Perret, and S. Tedjini, "A fully printable chipless RFID tag with detuning correction technique," *IEEE Microw. Wireless Compon. Lett.*, vol. 22, no. 4, pp. 209–211, 2012.
- [31] —, "Design of compact and auto-compensated single-layer chipless RFID tag," *IEEE Trans. Microw. Theory Tech.*, vol. 60, no. 9, pp. 2913–2924, 2012.
- [32] dupont.com. (2021). [accessed 01 mar. 2021]. [Online]. Available: <https://www.dupont.com/content/dam/dupont/amer/us/en/products/ei-transformation/documents/EI-10142-Kapton-Summary-of-Properties.pdf>



**Florian Requena** received the M.Sc. degree in electrical engineering from the Institut National Polytechnique de Grenoble, Valence, France, in 2019. He is currently a PhD student with the Institut National Polytechnique de Grenoble at the LCIS laboratory. His current scientific interests include chipless RFID and RF sensors.



**Nicolas Barbot** received the M.Sc. degree and Ph.D. degree from the Université de Limoges, France. His Ph.D. work in Xlim laboratory was focused on error-correcting codes for the optical wireless channel. He also realized a post-doctoral work in joint source-channel decoding at the LSS laboratory, in Gif-sur-Yvette, France. Since September 2014, he has been an Assistant Professor at the Université Grenoble Alpes - Grenoble Institute of Technology, in Valence, France. His research interest at LCIS laboratory includes backscattering communications, RFID and

Chipless RFID. More recently, he investigates the use of chipless tag as low-cost, batteryless and robust sensors.



**Darine Kaddour** (Member, IEEE) was born in Mechmech, Lebanon, in February 1982. She received the B.S. degree in physics from the Faculty of Sciences, Lebanese University, Tripoli, Lebanon, in 2003, and the M.S. and Ph.D. degrees from the Institut National Polytechnique de Grenoble, Grenoble, France, in 2004 and 2007, respectively. Since 2009, she has been an Assistant Professor with LCIS, where her research includes microwave circuits and RFID antennas.



**Etienne Perret** (S'02–M'06–SM'13) received the Eng. Dipl. degree in electrical engineering from the Ecole Nationale Supérieure d'Electronique, d'Electrotechnique, d'Informatique, d'Hydraulique, et des Télécommunications, Toulouse, France, 2002, and the M.Sc. and Ph.D. degrees in electrical engineering from the Toulouse Institute of Technology, Toulouse, in 2002 and 2005, respectively. From 2005 to 2006, he held a post-doctoral position with the Institute of Fundamental Electronics, Orsay, France. In 2006, he was appointed Associate Professor of

electrical engineering at Grenoble INP - Institute of Engineering Univ. Grenoble Alpes, France. From 2014 to 2019, he has been a Junior Member with the Institut Universitaire de France, Paris, France, an institution that distinguishes professors for their research excellence, as evidenced by their international recognition. From 2015 to 2020, he has been an Appointed Member of the French National Council of Universities. He has authored or co-authored more than 200 technical conferences, letters and journal papers, and books and book chapters. He holds several patents. His works have generated more than 3300 citations. His current research interests include electromagnetic modeling of passive devices for millimeter and submillimeter-wave applications, and wireless communications, especially RFID and chipless RFID, and also include advanced computer-aided design techniques based on the development of an automated codesign synthesis computational approach. Dr. Perret is a Technical Program Committee member of the IEEE International Conference on RFID, the IEEE RFID TA; and a member of the IMS Technical Paper Review Committee. He was a recipient of several awards like the MIT Technology Review's French Innovator's under 35 in 2013, the French Innovative Techniques for the Environment Award in 2013, the SEE/IEEE Leon Brillouin Award for his outstanding achievement in the identification of an object in an unknown environment using a chipless label or tag in 2016, the IEEE MTT-S 2019 Outstanding Young Engineer Award and the Prix Espoir IMT – Académie des sciences in 2020. He was a Keynote Speaker and the Chairman of several international symposiums. Etienne Perret was awarded an ERC Consolidator Grant in 2017 for his project ScattererID.